Conformational changes in a pore-forming region underlie voltage-dependent "loop gating" of an unapposed connexin hemichannel

Qingxiu Tang,[1] Terry L. Dowd,[2] Vytas K. Verselis,[1] and Thaddeus A. Bargiello[1]

[1]Dominic P. Purpura Department of Neuroscience, Albert Einstein College of Medicine, Bronx, NY 10461
[2]Department of Chemistry, Brooklyn College of the City University of New York, Brooklyn, NY 11210

The structure of the pore is critical to understanding the molecular mechanisms underlying selective permeation and voltage-dependent gating of channels formed by the connexin gene family. Here, we describe a portion of the pore structure of unapposed hemichannels formed by a Cx32 chimera, Cx32*Cx43E1, in which the first extracellular loop (E1) of Cx32 is replaced with the E1 of Cx43. Cysteine substitutions of two residues, V38 and G45, located in the vicinity of the border of the first transmembrane (TM) domain (TM1) and E1 are shown to react with the thiol modification reagent, MTSEA–biotin-X, when the channel resides in the open state. Cysteine substitutions of flanking residues A40 and A43 do not react with MTSEA–biotin-X when the channel resides in the open state, but they react with dibromobimane when the unapposed hemichannels are closed by the voltage-dependent "loop-gating" mechanism. Cysteine substitutions of residues V37 and A39 do not appear to be modified in either state. Furthermore, we demonstrate that A43C channels form a high affinity Cd^{2+} site that locks the channel in the loop-gated closed state. Biochemical assays demonstrate that A43C can also form disulfide bonds when oocytes are cultured under conditions that favor channel closure. A40C channels are also sensitive to micromolar Cd^{2+} concentrations when closed by loop gating, but with substantially lower affinity than A43C. We propose that the voltage-dependent loop-gating mechanism for Cx32*Cx43E1 unapposed hemichannels involves a conformational change in the TM1/E1 region that involves a rotation of TM1 and an inward tilt of either each of the six connexin subunits or TM1 domains.

INTRODUCTION

Although there is general agreement concerning the membrane topology of channels formed by the connexin gene family, there is considerable controversy concerning which of the four transmembrane (TM) helices and two extracellular loops are involved in pore formation as well as the organization of the remaining TM segments (for review see Yeager and Harris, 2007 and Verselis, 2009). A hemichannel or connexon is formed as a hexamer of an integral membrane protein (connexin) that spans the membrane four times with two extracellular loops (E1 and E2) and intracellular amino (NT) and carboxy termini. Based on an improved, but still low, 5.7 Å in plane and 19.8-Å vertical resolution cyroEM structure of Cx43 intercellular channels (Unger et al., 1999), Fleishman et al. (2004) constructed a computational Cα model of the structure of Cx32 gap junctions in which the third TM helix (TM3) formed the majority of the channel pore. Using a combination of molecular modeling and molecular dynamics, Pantano et al. (2008) refined this model to provide a fully atomistic representation of the Cx32 hemichannel. In this model, TM3 formed the majority of the pore in the TM region with the narrowest point of the pore at residue Y151 located in TM3 near the border of the second extracellular loop (E2). Furthermore, this model depicts E2 as forming most of the pore at the extracellular entrance of the hemichannel.

The assignment of TM3 as the major pore-lining helix is partially consistent with the experimental data of Skerrett et al. (2002). This study determined the accessibility of cysteine substitutions to the thiol modification reagent maleimidobutyryl biocytin (MBB) in macroscopic recordings of Cx32 intercellular channels formed in paired *Xenopus* oocytes in which one oocyte was cut open. The authors concluded that TM3 was the major pore-forming helix when the channel resided in the open state with a minor contribution of TM2 at the cytoplasmic end of the pore. Notably, MBB treatment of Y151C channels, which Pantano et al. (2008) model as the narrowest part of the pore, had only a small effect, surprisingly increasing rather than decreasing macroscopic conductance by ~10%. Residues in TM1 were proposed to enter the channel pore when the channel resided in the closed state. In contrast, Kronengold et al. (2003)

Correspondence to Thaddeus A. Bargiello: bargiell@aecom.yu.edu

Abbreviations used in this paper: bBBr, dibromobimane; DTT, dithiothreitol; MBB, maleimidobutyryl biocytin; MTS, methanthiosulfonate; NT, N terminus; TCEP, Tris(2-carboxyethyl) phosphine; TM, transmembrane; TPEN, *N,N,N′,N′*-tetrakis-(2-pyridylmethyl)-ethylenediamine; WT, wild-type.

The Rockefeller University Press $30.00
J. Gen. Physiol. Vol. 133 No. 6 555–570
www.jgp.org/cgi/doi/10.1085/jgp.200910207

demonstrated, with single-channel studies of Cx46 unapposed hemichannels, that residues located in the first TM helix (TM1) and first extracellular loop (E1) were modified by several methanthiosulfonate (MTS) reagents when the channel resided in the open state (see Fig. 10 A). There was no evidence of modification of residues in the second half of TM3 that would be pore lining in the atomistic model of Pantano et al. (2008) and were assigned to be pore lining by Skerrett et al. (2002). Modification of residues at two positions, I33C and M34C in TM1 of Cx32*Cx43E1, a Cx32 chimera in which E1 of Cx32 is replaced by that of Cx43, and I34C and L35C in Cx46 unapposed hemichannels with MBB, was reported by Zhou et al. (1997). These two studies implicate TM1/E1 rather than TM3/E2 as pore forming in Cx46 and Cx32*Cx43E1 unapposed hemichannels. Oh et al. (2008) reported modification of the T8C residue, which is located in the NT of unapposed hemichannels formed by Cx32*Cx43E1. Several studies have established the likelihood that the NT of Cx32 forms a vestibule at the intracellular entry of both the intercellular channel and unapposed Cx32*Cx43E1 hemichannel (Verselis et al., 1994; Oh et al., 2000, 2004, 2008; Purnick et al., 2000a,b). Collectively, studies of unapposed hemichannels implicate residues in NT, TM1, and E1 as contributors to the pore lining of connexin channels (for review see Verselis, 2009).

Knowledge of the structure of the connexin channel pore is not only essential to understand the selective permeation of connexin channels, but also to elucidate the molecular mechanisms of transjunctional (V_j) voltage gating. Harris et al. (1981) were the first to ascertain that the transjunctional voltage sensors of connexin channels must lie within the aqueous pore rather than in separate domains as exemplified by the superfamily comprising voltage-gated sodium, potassium, and calcium channels (Bezanilla, 2000; Tombola et al., 2006). They reasoned that the difference in the membrane potential of two coupled cells, V_j, would manifest itself as a voltage gradient along the length of the connexin channel pore. Because voltage gating in response to V_j depends only on the relative difference in potential of the two cells and not the absolute membrane potential, charged amino acids that form the voltage sensor must reside in the pore lining of connexin channels (see also Bargiello and Brink, 2009).

All vertebrate gap junctions display sensitivity to V_j. Two distinct mechanisms of V_j dependence have been described in both intercellular and unapposed hemichannels. These have been termed "V_j" or "fast" gating and "loop" or "slow" gating. In single-channel records, V_j or fast gating corresponds to fast transitions between the open state and at least one of three distinct subconductance states, whereas loop or slow gating involves a series of small amplitude transitions that link the open and a fully closed state. Consequently, channel closure by "loop gating" gives the appearance of a complex gating event with a measurable time constant (Trexler et al., 1996; Oh et al., 2000). At least a portion of the voltage sensor for the V_j gate resides in the NT of Cx32 and Cx26, and charged residues at the TM1/E1 border may also be involved (Verselis et al., 1994; Oh et al., 2000). The polarity of V_j gating of Cx32 and Cx26 hemichannels can be reversed by the addition of negatively or positively charged amino acids at several positions within the first 10 amino acids of the NT (Verselis et al., 1994; Purnick et al., 2000b; Oh et al., 2004), and it appears that "V_j gating" results from the individual movement of the six connexin subunits rather than a concerted movement of all six subunits (Oh et al., 2000). It has been proposed that V_j gating transitions might involve changes in the conformation of a proline kink motif in TM2 (Suchyna et al., 1993; Ri et al., 1999). Nothing is known about the location of the voltage sensor or changes in conformation underlying loop or slow voltage-dependent gating in unopposed Cx32*Cx43E1 hemichannels.

Here, we report that the pore structure of the unapposed Cx32*Cx43E1 hemichannel is very similar if not identical to that of Cx46 and Cx50 unapposed hemichannels in the vicinity of the TM1/E1 border. Furthermore, we demonstrate that the cysteine substitution of residue A43 located at the TM1/E1 border forms a high affinity cadmium binding site only when the channel resides in a closed conformation resulting from voltage-dependent loop gating, and that A43C residues can form homotypic disulphide bonds when oocytes are cultured in bath solutions containing 5 mM Ca^{2+}, a condition that favors channel closure. A40C residues also bind Cd^{2+} when the channel is closed by loop gating but with apparently much lower affinity than A43C channels. We propose that the mechanism of loop-gating closure of Cx32*Cx43E1 unapposed hemichannels involves a rotation of TM1/E1 and an inward tilt either of each connexin subunit or each TM1 helix.

MATERIALS AND METHODS

Site-directed mutagenesis, RNA synthesis, and oocyte injection

Site-directed point mutations were constructed using oligonucleotide primers (Gene Link) and the quick-change method (Agilent Technologies). All mutations were cloned into the plasmid vector pGEM-7ZF$^+$ (Promega) and sequenced. RNA was transcribed by using the Message-Machine kit with T7 RNA polymerase (Applied Biosystems) according to the manufacturer's instructions. 50 nl of ~1 ng/nl RNA was injected into each *Xenopus* oocyte obtained from *Xenopus laevis* (*Xenopus* 1) by standard procedures. After RNA injection, oocytes were cultured at 16°C in ND96 solution containing (in mM): 88 NaCl, 1 KCl, 5 $CaCl_2$, 1 $MgCl_2$, 10 HEPES, 2.5 pyruvate, and 0.1% glucose, pH 7.6.

Membrane protein purification and Western blots

Membrane proteins from 20 oocytes, cultured in ND96 containing 5 mM $CaCl_2$, were labeled with NHS-PC-LC-Biotin and purified

with a NeutroAvidin column according to the manufacturer's suggested procedure (Thermo Fisher Scientific). Proteins were released from the avidin column by treatment with 10% SDS and separated by SDS-PAGE through 4–20% Tris-glycine gradient gels (Invitrogen). After SDS-PAGE, proteins were transferred to PVDF membrane (Millipore) by semidry electro blotting (Owl Apparatus). Connexin proteins were localized with anti-Cx32 monoclonal antibody (Sigma-Aldrich) with a WesternBreeze Chromogenic Western Blot Immunodetection kit (Invitrogen).

Electrophysiological recording

Macroscopic oocyte membrane currents were recorded from *Xenopus* oocytes placed in an RC-1Z recording chamber (Warner Instruments). The basic bath solution contained (in mM): 100 CsOH–methanesulphonic acid, 1.8 $CaCl_2$, and 10 HEPES, pH 7.6. Additional reagents were added to this solution to the concentrations stated in the text. Dibromobimane (bBBr; Invitrogen) was dissolved in DMSO and diluted to the desired concentration. Gravity perfusion with suction was used to exchange bathing solutions. The volume of the chamber was 1.0 ml. Recording pipettes contained 3 M KCl and 10 mM HEPES, pH 7.6. A 3-M KCl agarose bridge connected the recording chamber to a ground chamber containing 3 M KCl and 10 mM HEPES, pH 7.6. Recordings were performed using either a GeneClamp 500 voltage clamp (MDS Analytical Technologies) or CA-1B high performance oocyte clamp (Dagan Instruments). Macroscopic currents were obtained at a sampling frequency of 5 kHz, filtered at 200 Hz, and when necessary decimated 50-fold for presentation.

Single-channel currents were recorded as described by Oh et al. (2000, 2004). MTSEA–biotin-X (2-((6-((biotinoyl)amino)hexanoyl)amino) ethylmethanethiosulfonate)) was purchased from Biotium, Inc., dissolved in DMSO (Sigma Chemical) to a stock concentration of 250 mM, and kept on ice before further dilution. Dilutions were made to a final concentration of 1 or 0.5 mM in bath solution just before bath application.

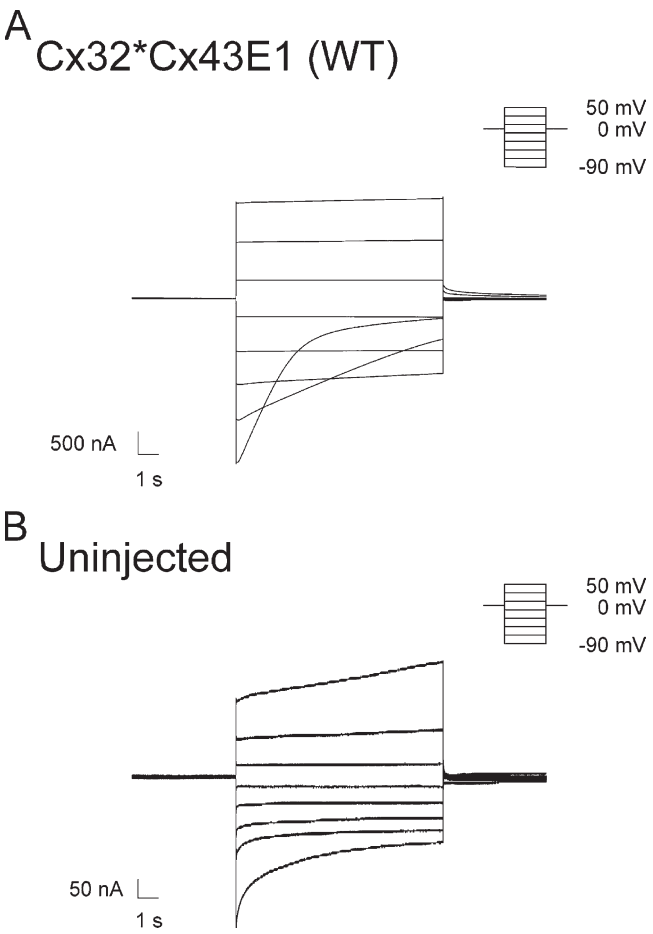

Figure 1. (A) Macroscopic current traces obtained from WT Cx32*Cx43E1 unapposed hemichannels after polarizations in 20-mV increments between −90 and 50 mV from a holding potential of 0 mV. The small increase in current level at large positive voltages results from the activation of an endogenous oocyte channel as assessed by recording uninjected oocytes. (B) Macroscopic current traces obtained from an uninjected oocyte illustrating typical endogenous currents present in oocytes obtained from *Xenopus* 1 frogs in Cs-MES bath solutions. There is variability in the form and magnitude of endogenous currents among oocytes, but in most cases endogenous currents contribute <300 nA.

RESULTS

With the exception of E41C, S42C, and W44C, unapposed Cx32*Cx43E1 hemichannels containing individual cysteine substitutions at residues V37 through G45 display voltage-dependent changes in macroscopic conductance that are qualitatively similar to that of the parental Cx32*Cx43E1 channel. Fig. 1 A illustrates a family of current traces obtained from an oocyte expressing Cx32*Cx43E1 that were elicited by a series of voltage polarizations from a holding potential of 0 mV. As reported by Oh et al. (2000), the relaxation of current that is observed at hyperpolarizing potentials results from the closure of either the loop and/or V_j gates. Cx32*Cx43E1 channels reside primarily in the open state at voltages more positive than −40 mV.

Macroscopic currents elicited by voltage for both E41C and S42C are too small (usually <300 nA) to be analyzed with confidence due to the expression of endogenous oocyte currents. Fig. 2 B illustrates a family of current traces elicited by a series of voltage polarizations from a holding potential of 0 mV that were obtained from an uninjected oocyte. Low levels of membrane insertion of E41C and S42C were confirmed by Western blots (not depicted). No macroscopic currents attributable to connexin hemichannels are evident after injection of W44C RNA. Membrane insertion of W44C by Western blotting was not examined.

Accessibility of cysteine substitutions to MTSEA–biotin-X

Fig. 2 shows that cysteine substitutions of V38 and G45 residues are accessible to modification with MTSEA–biotin-X when the Cx32*Cx43E1 channel resides in the open state and when the sulfhydryl reagent is applied from either the intracellular or extracellular side of the channel pore by addition to the bath solution. The stepwise reductions in current shown in this figure are not reversed by the removal of MTSEA–biotin-X by washing with bath solution, consistent with chemical modification of the cysteine residue.

Fig. 2 A illustrates an inside-out patch clamp recording of two G45C channels after the application of MTSEA–biotin-X. When the channel resides in the open state, 9 of a possible 12 stepwise reductions in current are observed. Based on the assumption that each step reflects a reaction between a single cysteine residue and the MTS reagent, it appears that at least five G45C residues are accessible to modification when the reagent is applied to the intercellular side of the channel pore. Fig. 2 B illustrates comparable modification of G45C residues in an outside-out recording of a single active channel. In this patch, five stepwise reductions in conductance are observed when the channel resides in the open state. This result shows that at least five of six G45C residues can be modified when the sulfhydryl reagent is applied to the extracellular side of the channel pore.

Fig. 2 C illustrates a record of an inside-out patch containing a single V38C channel. Again, this record shows that the V38C channel is accessible to modification when the channel resides in the open state and when the reagent is applied to the intracellular side of the channel pore. In this case, there are four stepwise changes in conductance, indicating that at least cysteine residues in four of six subunits are modified. Fig. 2 D

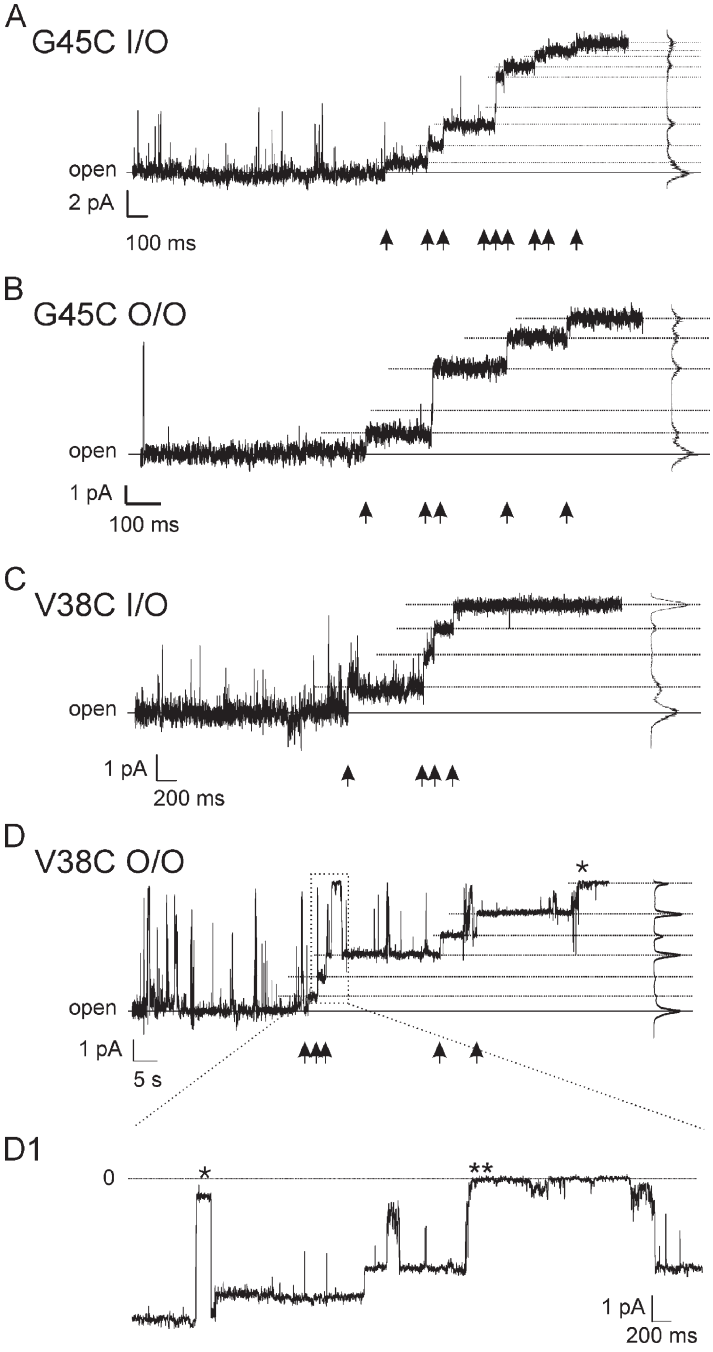

Figure 2. G45C and V38C residues are modified by MTSEA–biotin-X. Segments of patch clamp records of G45C and V38C after the addition of MTSEA–biotin-X to the bath solution at a final concentration of 1 or 0.5 mM. Arrows at the bottom of each panel mark step changes in conductance that are consistent with the reaction of a cysteine residue with MTSEA–biotin-X. Changes in current levels were determined with the all-point histograms shown on the right side of each panel. (A) Inside-out recording of two G45C channels. Nine conductance changes are evident, consistent with modification of 9 of 12 available G45C residues. The first modification event occurred 20 s after the bath application of 1 mM MTSEA–biotin-X. (B) Outside-out recording of a single G45C channel illustrating five conductance changes, consistent with modification of five of six available cysteine residues. The first modification event occurred 6 s after the bath application of 1 mM MTSEA–biotin-X. (C) Inside-out recording of a single V38C channel illustrating four conductance changes consistent with modification of four of six available subunits. The first modification event occurred 18 s after the bath application of 1 mM MTSEA–biotin-X. (D) Outside-out recording of a single V38C channel illustrating six conductance changes. It is not clear if the final conductance change, marked by an asterisk, resulted from a reaction, gating event, or channel loss; thus, at least five of six cysteine residues are modified. The first modification event occurred 64 s after the bath application of 0.5 mM MTSEA–biotin-X. The longer time to the first modification event correlates with the lower concentration of MTSEA–biotin-X used in this record (0.5 mM vs. 1.0 mM) than was used in the previous records. (D1) This is an enlargement of the boxed region of D. The event marked by the single asterisk is a V_J-gating transition that occurred after modification of two cysteine residues. The event marked by two asterisks is a loop-gating transition that occurred after three cysteine subunits were modified by MTSEA–biotin-X. Note that the loop- or slow-gating event involves a series of small amplitude transitions giving the appearance of a complex gating event with a measurable time constant, whereas the V_J-gating event occurs as a single fast step between the open state and a subconductance state. Zero current level indicated by the dashed line is the leak-subtracted current.

demonstrates the modification of V38C residues in a single channel recording obtained in the outside-out configuration. In addition, the record illustrates that both V_j and loop gates are operational when two and three subunits are modified, respectively, by MTSEA–biotin-X. In the enlarged section of the trace, Fig. 2 D1, the channel undergoes a V_j-gating transition (marked by an asterisk) after two stepwise reductions in conductance and shortly after reopening a third modification occurs. Shortly thereafter, the channel undergoes a loop-gating event (marked by two asterisks) that appears to result in full channel closure. After reopening from the fully closed state, two additional stepwise changes in conductance are observed that are consistent with modification of the remaining two subunits (Fig. 2 D). It is not clear if the final step (marked by the asterisk in Fig. 2 D) resulted from a modification, gating event, or channel loss, as the resulting conductance is similar to that of complete channel closure by loop gating. Consequently, we conclude that at least five of six cysteine residues are modified. No modifications were observed or can be inferred to have occurred when the V38C channel resided although briefly in either the V_j- or loop-gated closed conformation. In all cases, removal of unreacted MTSEA–biotin-X by washing with bath solution had no effect on the conductance of reacted channels.

There is no evidence that MTSEA–biotin-X modifies the open state of channels formed by cysteine substitutions at residues A40 and A43 as assessed by single-channel recording of excised patches (not depicted). No modification was apparent in macroscopic recordings of V37C and A39C channels at hyperpolarizing or depolarizing potentials (not depicted). The accessibility of these residues to MTSEA–biotin-X was not examined in excised patches. Low or lack of expression precluded examination of modification of channels formed by E41C, S42C, and W44C.

We conclude that residues V38C and G45C line the aqueous pore of the open Cx32*Cx43E1 unapposed hemichannel, whereas residues V37C, A39C, A40C, and A43C do not appear to be accessible to thiol modification when the channel resides in the open state.

Effects of DTT, TPEN, and TCEP on membrane currents produced by A43C

Typically, oocytes injected with A43C RNA display low levels of current when examined 1–2 d after injection. Given that A43C residues do not appear to line the pore of the open channel, this observation suggested a possible interaction among the substituted cysteine residues that may involve disulfide bond formation or interactions with divalent metal ions when the channel resides in a closed state. These possibilities were explored by examining the effects of disulphide bond reducing agents and transition metal chelators on A43C membrane currents.

Treatment of A43C oocytes, displaying small initial currents, with low concentrations of dithiothreitol (DTT; 20 μM), results in a rapid and large increase in membrane current (Fig. 3) that is attributable to the activation of connexin hemichannels already inserted into the oocyte membrane. In the case shown, currents attributable to A43C unapposed hemichannels increase fivefold after the application of DTT. Overall, the efficacy of DTT to increase currents was variable, ranging from a small effect to a 10-fold increase ($n = 77$ oocytes). The variability in the effect of DTT roughly correlates with the time

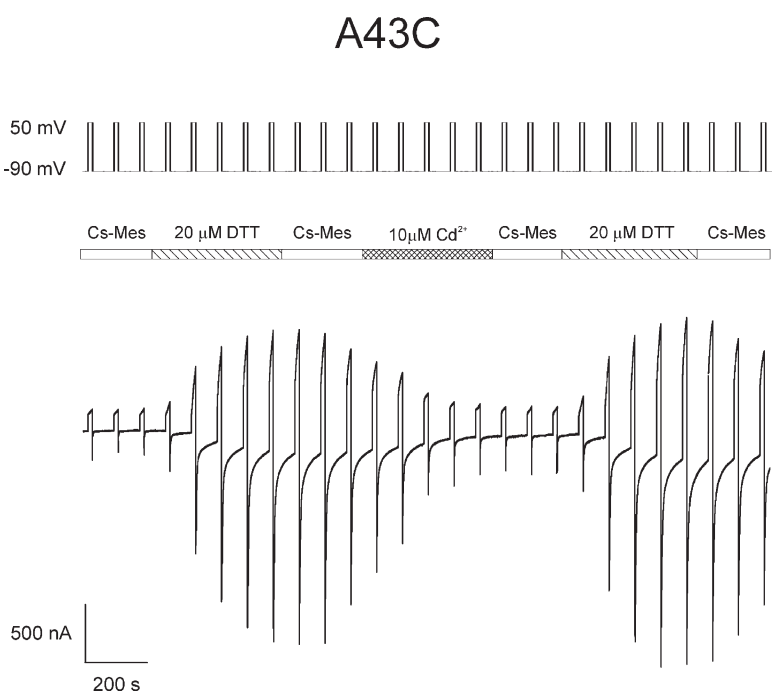

Figure 3. DTT and cadmium alter levels of A43C currents. Macroscopic currents elicited from an oocyte expressing A43C unapposed hemichannels with the voltage paradigm shown at the top of the panel. The central bar indicates the time and duration at which the bath solution containing 100 mM Cs-MES, 1.8 mM $CaCl_2$, and 10 mM HEPES, pH 7.6, was exchanged with the same bath solution except containing either 20 μM DTT or 10 μM $CdCl_2$. Currents increased to a steady-state level approximately fivefold greater than the initial currents after exposure to 20 μM DTT and decreased to ~80% of maximum after treatment with 10 μM $CdCl_2$. The reduction in current was not changed substantially by washing with the bath solution but was reversed to pre-cadmium levels after wash with 20 μM DTT.

interval between injection and recording. Generally, records obtained from oocytes 3–4 d after injection display larger initial A43C currents and a much smaller increase in current after treatment with DTT. Comparable increases of A43C currents can be obtained by treatment with 500 μM Tris(2-carboxyethyl) phosphine (TCEP), a membrane-impermeant reagent, suggesting that disulphide bond formation may underlie the attenuation of initial A43C currents. However, 10 μM *N,N,N′,N′*-tetrakis-(2-pyridylmethyl)-ethylenediamine (TPEN), a membrane-permeable transition metal chelator with a low affinity for Ca^{2+} and Mg^{2+} that does not reduce disulphide bonds, has an effect comparable to the two disulfide reducing agents. Application of DTT after TPEN treatment does not substantially increase A43C currents in most oocytes, but does so in a small percentage, suggesting an additional action of DTT in some cases. It should be noted that, in addition to reducing disulphide bonds, DTT can also chelate metal ions with high affinity (Krezel et al., 2001), whereas TCEP is a weaker chelator of metal ions (Krezel et al., 2003). Removal of DTT by extensive washing of oocytes expressing A43C is often accompanied by a slow reduction in current levels that can be reversed by subsequent treatment with DTT or TPEN (Fig. 3).

Increased currents in response to micromolar concentrations of DTT, TPEN, and TCEP are not observed in the parental Cx32*Cx43E1 channel nor in any other cysteine substitutions examined in this study (not depicted).

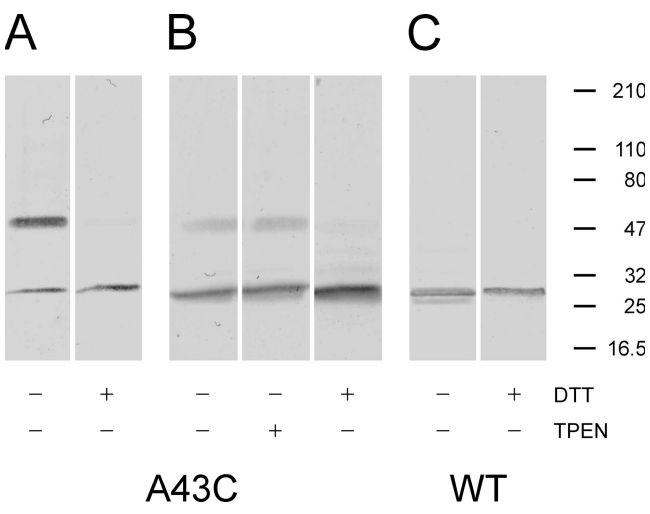

Figure 4. Western blots of WT (Cx32*Cx43E1) and mutant (A43C) membrane-inserted hemichannels. + and − symbols at the bottom of each panel denote treatment of the sample with or without either 50 mM DTT or 10 mM TPEN before SDS-electrophoresis through 5–40% gradient polyacrylamide gels. The position of pre-stained molecular weight standards (Thermo Fisher Scientific) are presented as bars on the right side of the figure. The band with molecular weight ∼50 kD corresponds to a connexin dimer, whereas the monomer has an electrophoretic mobility comparable to a molecular weight standard of ∼27 kD. Only treatment with DTT reduces the dimer to the monomeric connexin form.

Treatment of uninjected oocytes with 20–100 μM DTT, 10 μM TPEN, or 500 μM TCEP has little if no effect on the levels of endogenous oocyte currents.

Effect of cadmium on A43C membrane currents

The effect of TPEN and the absence of an additive effect of DTT, observed in most cases, suggest that chelation of transition metals rather than disulfide bond formation underlies the increase in A43C current. This possibility was explored further by examining the effect of cadmium, a soft, highly polarizable group IIB transition metal that can coordinate with cysteine residues, on A43C membrane current. Fig. 3 illustrates that DTT-treated A43C oocytes display a large reduction in current after wash with DTT-free solution and subsequent application of 10 μM Cd^{2+}. In the trace shown, current levels are reduced by >80% in the presence of 10 μM Cd^{2+} and are not restored by washing with Cd^{2+}-free solution for the time indicated. The residual currents are most likely a combination of endogenous oocyte currents and leak current, both of which are variable between oocyte batches and were not subtracted.

The reduction of A43C currents by cadmium is independent of the amount of current increase caused by DTT treatment. The average reduction with 10 μM Cd^{2+} is 73 ± 6% (n = 18). Treatment of A43C oocytes with 1 μM Cd^{2+} results in a 70 ±1% (n = 3) decrease in current. The similarity in the magnitude of inhibition at these concentrations suggests that the Cd^{2+} binding affinity is high. The connexin currents can only be restored to pre-Cd^{2+} levels by treatment with either 20 μM DTT, 10 μM TPEN, or 500 μM TCEP. Extensive washing with Cd^{2+}-free solutions has little effect on current levels with the duration of the wash used in this study. 10 μM Cd^{2+} has no effect on membrane currents attributable to parental Cx32*Cx43E1 channels or endogenous channels. 100 μM Cd^{2+} causes some reduction in parental currents, but the effect is readily and completely reversed after wash with Cd^{2+}-free solutions (not depicted).

Western blots indicate that A43C channels can form disulfide bonds

Although electrophysiological studies indicate that low levels of A43C currents observed 1–2 d after injection likely occur as a consequence of metal coordination, Western blots of membrane-inserted A43C channels cultured in ND96 media containing 5 mM Ca^{2+}, a concentration that strongly favors connexin hemichannel closure and appears to increase the survival time of injected oocytes presumably by reducing connexin membrane currents, demonstrate that disulfide bonds can form between neighboring A43C residues (Fig. 4). As shown in Fig. 4 A, ∼75–80% of connexin immunoreactivity is localized to a band whose molecular weight corresponds to that expected for a connexin dimer (54 kD), whereas the remainder corresponds to the lower molecular

weight monomer (27 kD). Treatment of the sample with 50 mM DTT shifts all immunoreactivity to the monomeric form. Notably, no molecular weight forms larger than dimers are observed in Western blots of homomeric A43C channels. Similar results were obtained in 3 of 30 Western blot experiments. In most cases (27 of 30 blots), the intensity of the dimer is less than that of the monomer, accounting for ~10–20% of the total immunoreactivity (Fig. 4 B). In this experiment, the dimer was reduced to the monomeric form after treatment with 50 mM DTT but was insensitive to treatment with 10 mM TPEN. Fig. 4 C illustrates a Western blot of parental Cx32*Cx43E1 membrane-inserted unapposed hemichannels. Only the connexin monomer is detected, and there is no change in mobility after DTT treatment. The results of the biochemical experiments indicate that disulfide bond formation may contribute in part to the reduced levels of A43C current, although in most cases it appears that binding of endogenous divalent metal ions, such as Cd^{2+}, have a larger effect.

State dependence of Cd^{2+} inhibition and bBBr modification of A43C residues

Fig. 5 A illustrates that the inhibition of A43C currents by micromolar concentrations of Cd^{2+} occurs at hyperpolarizing potentials that correlate with the voltage dependence of channel closure. Membrane currents are reduced to a steady-state level, ~85% of their DTT-treated value, after perfusion with 10 μM Cd^{2+} while the oocyte is repeatedly hyperpolarized by alternating steps between −90 and 0 mV. A similar reduction in current is observed when Cd^{2+} is applied to channels that had been closed in response to a long hyperpolarizing step to −90 mV, washed with Cd^{2+}-free solution, and tested with polarizations alternating between −90 and +50 mV (Fig. 5 B). In contrast, the application of 10 μM Cd^{2+} after moderate hyperpolarization to −20 mV (not depicted), or depolarization to 30 mV (Fig. 5 C), voltages that strongly favor open-channel residency, has little if no effect on current levels. This result suggests that Cd^{2+} binds to A43C residues when the channel resides in a closed state. The marked reduction of A43C current by Cd^{2+} at

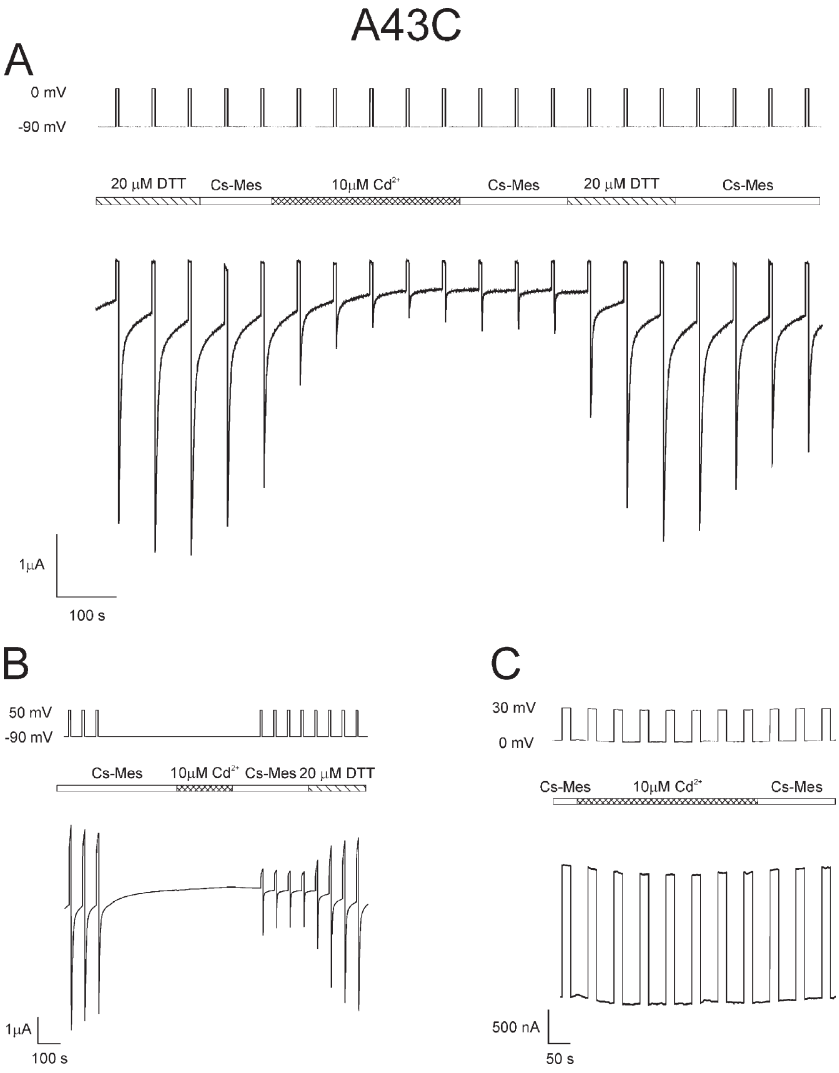

Figure 5. Cadmium locks A43C unapposed hemichannels in a closed state. (A) Macroscopic currents elicited from an oocyte expressing A43C unapposed hemichannels with the voltage paradigm, steps from −90 to 0 mV, shown at the top of the panel. The central bar indicates the time and duration for which the bath solution containing 100 mM Cs-MES, 1.8 mM $CaCl_2$, and 10 mM HEPES, pH 7.6, was exchanged with the same bath solution except containing either 20 μM DTT or 10 μM $CdCl_2$. Currents were decreased to ~85% of maximum levels after treatment with 10 μM $CdCl_2$. The reduction in current could only be reversed after a second exposure to 20 μM DTT. (B) 10 μM $CdCl_2$ was applied to the channel after a long-duration hyperpolarizing step that would favor closure of both loop and V_j gates. After wash with Cs-MES bath solution, the extent of current reduction was assessed by a series of polarizing steps between −90 and 50 mV. Currents were reduced by ~80% by Cd^{2+} treatment when the channels resided in a closed state. Currents could only be recovered fully after exposure to 20 μM DTT. (C) Macroscopic currents elicited from an oocyte expressing A43C unapposed hemichannels with the voltage paradigm, steps between 0 and 30 mV, which strongly favors population of the open-channel state. Application of 10 μM $CdCl_2$ had no effect on the level of A43C current, indicating that A43C residues do not coordinate Cd^{2+} when the channel resides in the open state.

large hyperpolarizing potentials can only be reversed after the application of 20 μM DTT (Fig. 5, A and B) or 10 μM TPEN (not depicted).

Irreversible reductions in current also result when A43C channels are exposed to the polar, thiol cross-linking reagent bBBr, with voltage paradigms that favor channel closure. This is illustrated in Fig. 6 A, where bBBr was applied during a series of hyperpolarizing steps to −90 mV from a holding potential of 0 mV. A43C currents are not decreased when this reagent is applied during depolarizing steps from 0 to 30 mV (Fig. 6 B), a voltage paradigm that maintains the channel in the open state. We did not attempt to verify that the reduction in current results from cross-linking neighboring A43C residues by examining changes in fluorescence intensity that are expected to occur if bBBr cross-linked neighboring cysteine residues (Kim and Raines, 1995). Thus, it is possible that the reduction in current was due to the modification of individual thiols rather than cross-linking of neighboring thiol groups. However, regardless of the mechanism underlying the observed current reduction, the correlation between the voltage dependence of channel closure and inhibition of A43C current by bBBr indicates that A43C residues are accessible to modification only when the channel resides in a closed conformation. bBBr has no effect on Cx32*Cx43E1 currents or those present in uninjected oocytes (not depicted).

Cd^{2+} inhibition of heteromeric A43C/wild-type (WT) channels

The reduction of A43C currents by Cd^{2+} could in principle arise from interactions between a single cysteine residue and single Cd^{2+} ion (i.e., a lower affinity monodentate interaction) or by the formation of a dative covalent bond (coordination) involving a single Cd^{2+} ion and multiple cysteine residues (i.e., a higher affinity polydentate interaction). To further examine the molecular basis for the reduction in A43C currents by Cd^{2+}, we examined the efficacy of Cd^{2+} current reduction and recovery after wash in heteromeric channels formed by coinjection of A43C and WT RNA.

Currents attributable to heteromeric channels formed by coinjection of equal amounts of A43C and WT Cx32*Cx43E1 RNA are less sensitive to inhibition by 10 μM Cd^{2+} after initial treatment with 20 μM DTT and wash with Cs-MES bath solution than currents of homomeric A43C channels. With the 1:1 RNA ratio, currents are reduced by 58 ± 14% (n = 8), suggesting that fewer cysteine residues are available to bind cadmium and/or that the affinity of cadmium binding is reduced in heteromeric channels. The large variation in effect can be explained in part by variation in the expression among oocytes of endogenous currents that are not affected by Cd^{2+}. Notably, however, heteromeric channel currents that have been inhibited by treatment with 10 μM Cd^{2+} subsequent to DTT treatment and wash can be restored on average to ∼75 ± 5% (n = 4) of their initial values by washing with Cd^{2+}-free solution (Fig. 7 A). This suggests that ∼25% of heteromeric channels bind cadmium with high affinity. This measure of recovery is not influenced by variations in the levels of endogenous currents among

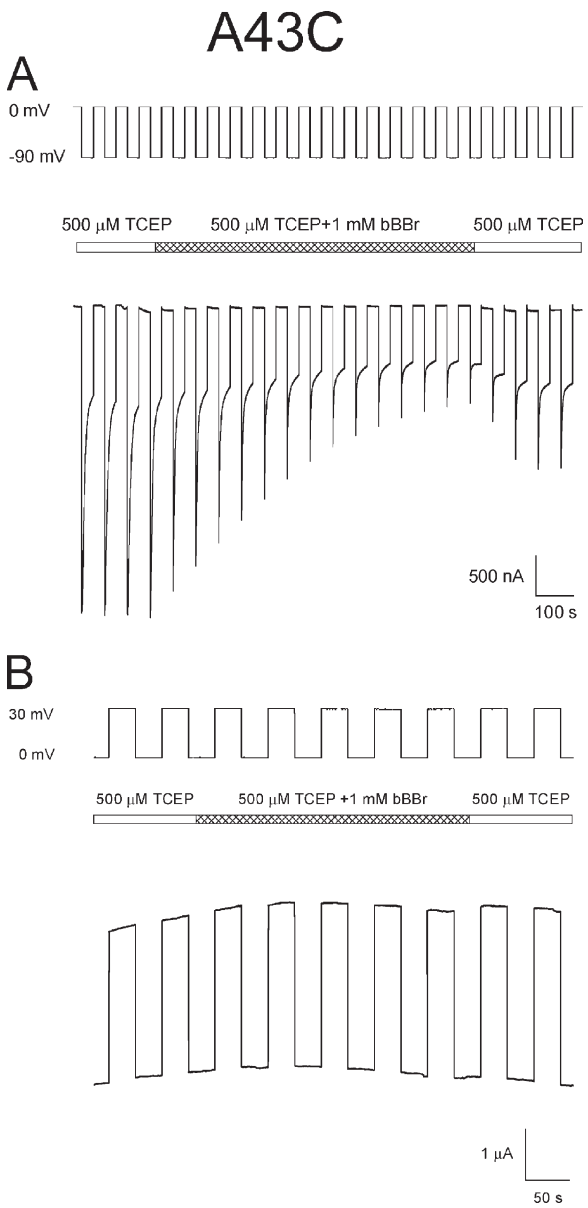

Figure 6. Modification of A43C residues by bBBr occurs at voltages that favor channel closure. (A) Macroscopic currents attributable to A43C channels are irreversibly decreased when exposed to bBBr during a voltage paradigm, steps between 0 and −90 mV, which elicits gating transitions between the open (0 mV) and either loop- and/or V_j-gating closed states (−90 mV). (B) Application of bBBr during a voltage paradigm, steps from 0 to 30 mV, which favors population of the open-channel state, has no effect on A43C macroscopic currents. The central bar in both panels indicates the time and duration for which the bath solution containing 500 μM TCEP was exchanged with the same bath solution containing 1 mM bBBr and subsequently washed with TCEP containing bath solution.

oocytes, and therefore provides a reliable estimate of the proportion of channels that bind Cd^{2+} with high affinity. As there is little or no difference in the kinetics of activation of currents in response to polarizations to 50 mV before, during, and after the application of Cd^{2+} (Fig. 7 B), the differences in current levels observed with the experimental paradigm used in Fig. 7 A cannot be ascribed to difference in the rates of channel activation.

Assuming that A43C and WT subunits are equally expressed and randomly assembled, 65% of channels are predicted by the binomial distribution to contain at least three A43C subunits, whereas 34% contain at least four A43C subunits, and 10% contain at least five A43C subunits when equal amounts of A43C and WT are injected. The percentage of channels estimated to contain a high affinity Cd^{2+} site (25%) is less than the number predicted to contain four or more subunits (34%), but greater than the number containing five or more subunits (10%), suggesting that at least four cysteine-containing subunits are involved. The deviation from the expected values suggests that the order of subunit arrangement in channels containing four cysteine subunits may be important in creating a high affinity site.

In the case of heteromeric channels formed by coinjection of four parts A43C RNA to one part Cx32*Cx43E1 RNA, the inhibition of current by 10 μM Cd^{2+} (~87 ± 8.7%; $n = 4$) is greater than that observed for 1:1 heteromeric channels, and currents are restored to 49 ± 8% ($n = 4$) of pre-Cd^{2+} levels by washing with Cd^{2+}-free solution (not depicted). In this case, 51% of channels are inferred to bind Cd^{2+} with high affinity, whereas 96% of channels are predicted to contain three or more cysteine subunits, 83% contain four or more A43C subunits, and 53% contain five or more

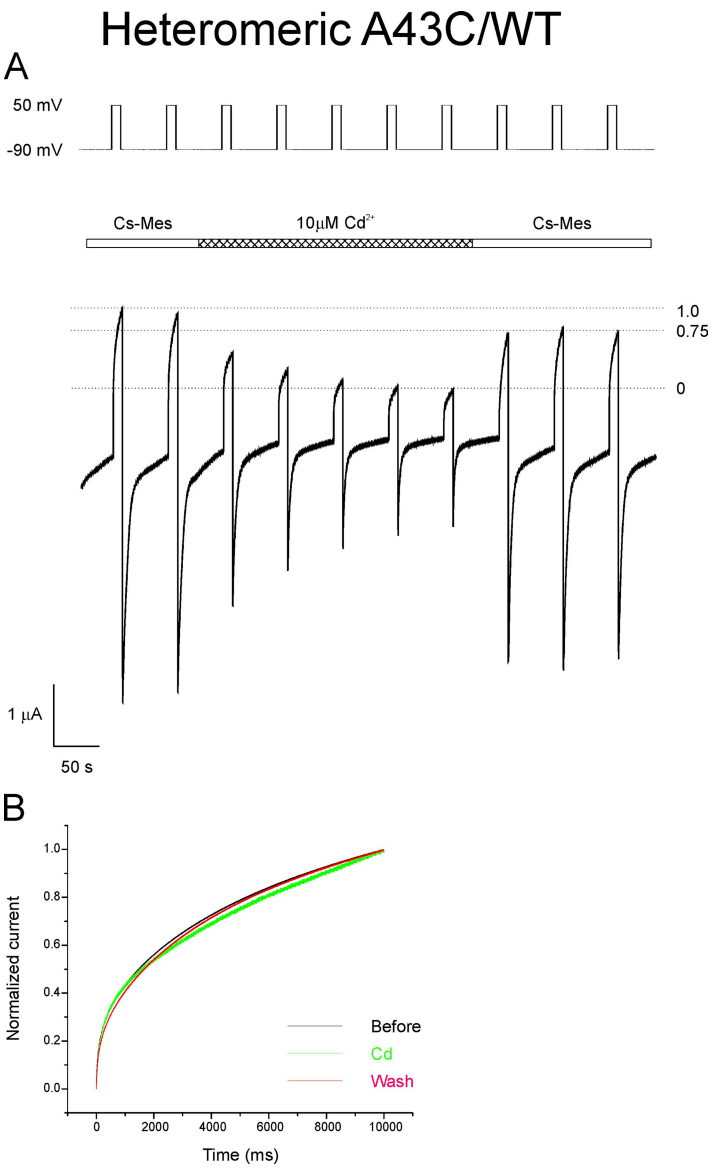

Figure 7. Effect of 10 μM $CdCl_2$ on heteromeric channels formed by coexpressing 1:1 mixtures of WT and A43C RNA. (A) Heteromeric channels were treated with 20 μM DTT and washed with Cs-MES, 1.8 mM Ca^{2+} bath solution before the application of Cd^{2+} shown in the trace segment. After the reduction of macroscopic currents by treatment with 10 μM $CdCl_2$, currents were restored to 75% of pre-cadmium levels by washing with cadmium-free bath solution. The result is interpreted to indicate that 25% of channels form a high affinity cadmium site that "locks" the channel in a closed conformation (see Results). (B) Comparison of the kinetics of channel activation upon depolarization to 50 mV before (black trace), during (green trace), and after (red trace) the application of Cd^{2+} in the trace shown in A. The two current traces before Cd^{2+} were averaged, as were the final two current traces after wash. The green trace is current trace obtained just before wash with Cd^{2+}-free solution. The similarity among normalized traces indicates that the differences in current levels are not a consequence of differences in the kinetics of activation, but most likely reflects the proportion of channels that can be activated by the voltage step.

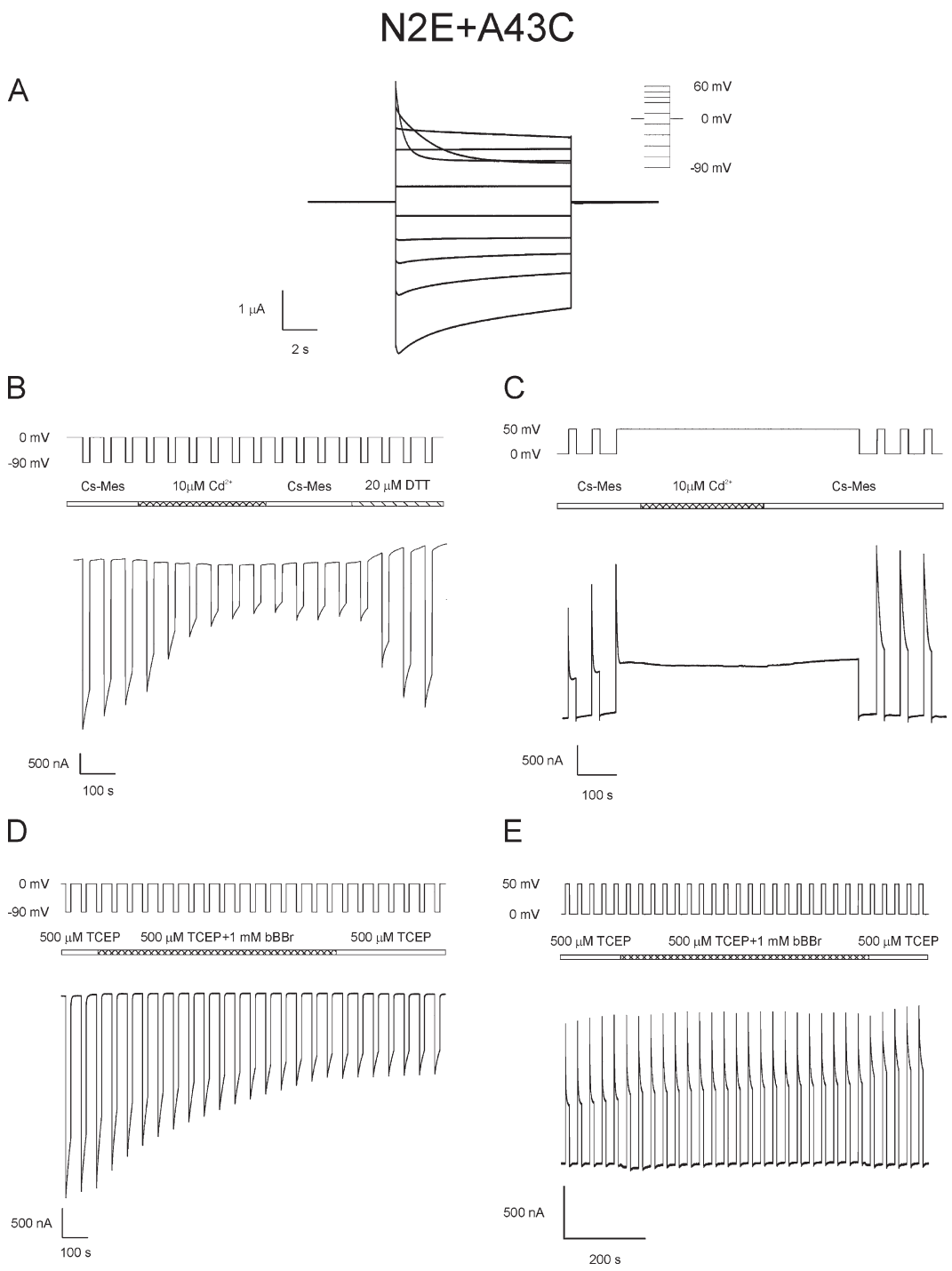

Figure 8. Unapposed N2E+A43C hemichannels are locked by cadmium and accessible to bBBr modification when the channel is closed by loop gating, but not V_j gating. (A) Macroscopic current traces obtained from N2E+A43C unapposed hemichannels after polarizations to voltages shown in the inset of 0 mV. Current relaxations at hyperpolarizing and depolarizing potentials result from the closure of loop and V_j gates, respectively. (B) Macroscopic currents were recorded from oocytes expressing the double mutation, N2E+A43C. The N2E mutation reverses the polarity of V_j gating from closure at hyperpolarizing potentials to closure at depolarizing potentials but does not change the polarity of loop gating. The application of 10 μM $CdCl_2$ during a series of voltage steps between 0 and −90 mV causes a large decrease in membrane currents that can only be reversed by treatment with 20 μM DTT. Polarizations to −90 mV strongly favor the closure of loop gates, whereas residency in the open state is favored at a holding potential of 0 mV. (C) Macroscopic currents recorded from N2E+A43C oocyte using a similar protocol to that used in Fig. 5 B. 10 μM $CdCl_2$ was applied to the channel after a long-duration depolarizing step to 50 mV that strongly favors closure of only the V_j gates. After wash with Cs-MES bath solution, the effect of cadmium on V_j gate closed channels was assessed by the application of a series of polarizing steps between 0 and 50 mV. This polarization elicits gating transitions between the open and V_j-gating closed states. Currents were similar to those obtained before cadmium application, demonstrating that A43C residues do not coordinate cadmium when the channel is closed by V_j gating. (D) Macroscopic current traces

A43C subunits. The percentage of channels that appear to form a high affinity Cd^{2+} site in the 4:1 RNA ratio (51%) is similar to the percentage of channels expected to contain at least five subunits. Collectively, the results from 1:1 and 4:1 RNA ratios imply that at least four A43C residues interact with cadmium and this in turn suggests that coordination of Cd^{2+} underlies the high cadmium affinity of A43C channels.

Cadmium coordination and thiol modification correlate with closure of "loop gates"

Polarization to −90 mV is sufficient to induce A43C channel closure by either one of two voltage-dependent mechanisms, V_j and/or loop gating. The ability of negative charge substitutions at the second amino acid residue to selectively reverse the polarity of V_j gate from closure favored at negative to closure favored at positive potentials (Oh et al., 2000) provides a means to determine if Cd^{2+} interacts with cysteine residues in channels closed by either the V_j and/or the loop gate.

In macroscopic recordings of N2E+A43C in bath solutions containing 1.8 mM Ca^{2+}, the voltage dependence of loop gating is shifted to smaller hyperpolarizing potentials relative to A43C channels. N2E+A43C channel closure by loop gating is observed at voltages equal to or more negative than −30 mV compared with closure of either the V_j or loop gates at voltages more negative than −50 mV for the parental Cx32*Cx43E1 channel. Current relaxations at depolarizing potentials are attributable to closure of the V_j gates (Fig. 8 A). The reversal of V_j gating polarity in the double mutation, Cx32*Cx43E1(N2E+A43C) unapposed hemichannels, from closure at negative potentials to closure at positive potentials was confirmed by single-channel recording (not depicted).

Fig. 8 B demonstrates that N2E+A43C channel currents are reduced substantially (∼70%) by 10 μM Cd^{2+} when the channel is repeatedly stepped from 0 to −90 mV, a voltage paradigm that favors closure of only the loop gates. On average, N2E+A43C currents are reduced by 62 ± 16% (n = 4), a reduction similar to that observed for A43C channels (73 ± 6%; n = 18). Reduction of N2E+A43C currents that can only be reversed by DTT or TPEN treatment is also observed when Cd^{2+} is applied to channels after depolarizing steps to −30 mV (not depicted), a voltage that correlates with the shift in voltage dependence of loop gating described above. This result supports the view that Cd^{2+} coordination occurs only when the loop gates reside in the closed conformation.

There is no evidence that Cd^{2+} is coordinated by A43C residues when N2E+A43C channels are closed by V_j gating. This is illustrated in Fig. 8 C, where the closure of the V_j gates is elicited by membrane depolarization to 50 mV. Subsequent application of 10 μM Cd^{2+} followed by wash with Cd^{2+}-free bath solution at this holding potential does not result in the reduction of N2E+A43C currents when tested by alternating voltage steps between 0 and 50 mV. We maintain that this is not a consequence of reduced concentration of Cd^{2+} at the A43C coordination site that is expected to occur as a consequence of the imposed positive voltage gradient that would tend to oppose Cd^{2+} entry into the channel, for the following reasons. First, similar results are obtained when 100 μM Cd^{2+} is applied in this protocol (not depicted). Recall that 100-fold less, i.e., 1 μM Cd^{2+}, causes a marked reduction in A43C currents when the channels are closed by loop gating. Second, given the expected proximity of A43C residue to the extracellular surface of the channel, the fraction of the electrical distance that would be traversed by Cd^{2+} to the coordination site is expected to be small. Consequently, it is likely that concentration of Cd^{2+} at a holding potential of 50 mV would be sufficient to lock the channel if A43C residues adopted a conformation capable of coordinating Cd^{2+} when the N2E+43C channel is closed by V_j gating. 10 μM Cd^{2+} has little or no effect on currents attributable to N2E channels (not depicted).

Currents were reduced on average by ∼42 ± 18% (n = 5) when N2E+A43C channels are closed by hyperpolarization to −90 mV in the presence of bBBr (Fig. 8 D). bBBr has no effect on N2E+A43C currents when the oocytes are stepped from 0 to 50 mV, a voltage that closes only the V_j gates (Fig. 8 E). We conclude that A43C residues coordinate cadmium ions and become accessible to bBBr modification when the channel is closed by loop gating, but not V_j gating.

DTT and cadmium effects on cysteine substitutions at other positions

In contrast to A43C, 20 μM DTT has no effect on unapposed hemichannels formed by A40C. However, 10 μM Cd^{2+} has a pronounced inhibitory effect, reducing A40C currents by 56 ± 20% (n = 12), but unlike A43C channels, the inhibition is readily reversed by washing with Cd^{2+}-free solutions (Fig. 9 A). bBBr irreversibly reduces A40C currents by 42 ± 7% (n = 3) when applied at potentials that are sufficient to close the loop gates of this channel (Fig. 9 B).

elicited by repeated polarizations between 0 and −90 mV, a voltage paradigm that elicits transitions between open and loop gate closed channels. At the position indicated, channels were exposed to 1 mM bBBr in the presence of 500 μM TCEP and subsequently washed with 500 μM TCEP. The observed reduction in current is consistent with a reaction between the A43C residue and bBBr. (E) Macroscopic current traces elicited by repeated polarizations between 0 and 50 mV, a voltage paradigm that results in the opening and closing of V_j gates. At the position indicated, channels were exposed to 1 mM bBBr in the presence of 500 μM TCEP and subsequently washed with 500 μM TCEP. The absence of any reduction in current is interpreted to indicate the inaccessibility of A43C residues to bBBr modification when the N2E+A43C channel resides in the open state and the V_j-gated closed state.

10 μM Cd^{2+} reduces currents slightly, ~20%, in channels formed by V38C and G45C, the two residues modified by MTSEA–biotin-X in the open state, but the reduction is readily reversible by washing with Cd^{2+}-free solutions, consistent with low affinity binding. 20 μM DTT has no effect on the initial currents of these channels. Unapposed hemichannels formed by cysteine substitutions at V37 and A39 are unaffected by the addition of 10 μM Cd^{2+} at both hyperpolarizing and depolarizing potentials, and initial currents are not changed after treatment with 20 μM DTT.

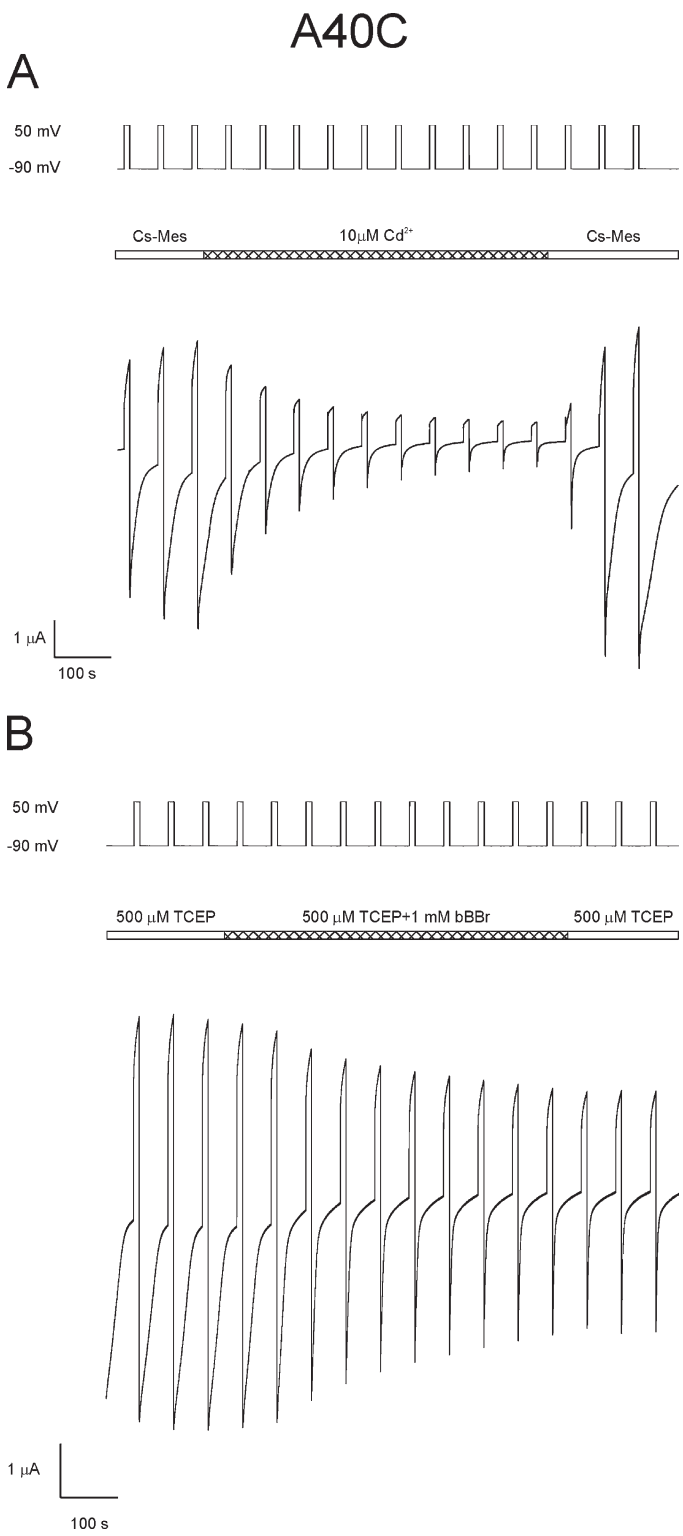

Figure 9. Cadmium and bBBr reduce A40C currents. (A) Reduction of A40C unapposed hemichannel currents by $CdCl_2$ is reversed by washing. Macroscopic currents attributable to A40C residues were examined by applying a series of voltage polarizations between −90 and 50 mV. The application of 10 μM $CdCl_2$ during this voltage paradigm causes a ~90% reduction in current in the case shown. However, unlike A43C channels, currents are fully restored by wash with cadmium-free bath solution. These results are interpreted to indicate that A40C residues do not form a high affinity cadmium binding site when the channel is closed by either loop or V_j gating. (B) A40C unapposed hemichannels are accessible to bBBr modification. BBBr was applied to the channels at the time indicated in the bar line as the channel was repeatedly stepped from −90 to 50 mV. Currents were reduced by ~50% at positive potentials and were not reversed by wash.

DISCUSSION

The structure of the open channel in the vicinity of the M1/E1 border

The data presented here demonstrate that cysteine substitutions at two residues, V38 and G45, which are located near the M1/E1 border of the unapposed Cx32*Cx43E1 hemichannel, are modified by MTSEA–biotin-X when the channel resides in the open state. Furthermore, the accessibility of these residues to modification by the membrane-impermeant MTSEA–biotin-X from either the cytoplasmic or intracellular entry of the channel indicates that these residues most likely reside in the channel pore rather than within a crevice in the protein core or within a crevice at the protein–lipid interface.

There is no evidence that cysteine substitutions of residues V37, A39, A40, and A43 are modified by MTSEA–biotin-X when the channel resides in the open state. Membrane currents attributable to V37C and A39C channels are not decreased by low concentrations of Cd^{2+}, nor are currents of these channels increased after the application of DTT or TPEN. We conclude that residues V37, A39, A40, and A43 do not line the aqueous pore of the open channel, but rather, that they are likely to be buried within the protein core of the unapposed hemichannel.

The overall pattern of accessibility of cysteine substitutions of residues 37–45 in Cx32*Cx43E1 matches that reported for the open unapposed Cx46 hemichannel by Kronengold et al. (2003) and Cx50 (Verselis et al., 2009). Fig. 10 A shows a helical wheel representation of residues R33 through G46 of Cx46. Reacted residues, shown in red, subtend an arc of ~80° on one side of the helix, and based on the accessibility of the open state of channels formed by these residues to MTS reagents, Kronengold et al. (2003) conclude that they line the pore of the open Cx46 unapposed hemichannel. The homologous residues of Cx32*Cx43E1 are superimposed on the helical wheel in Fig. 10 B and indicate that residues V38, S42, and G45 are predicted to line the aqueous pore. We have confirmed that residues V38 and G45 most likely line the pore of the open channel based on their reactivity to the membrane-impermeant MTSEA–biotin-X from both sides of the channel pore. The predicted accessibility of S42C to thiol modification could not be tested due to low expression of this mutation. We did not examine the accessibility of M34C. Modification of this residue by MBB in Cx32*Cx43E1 channels has been reported by Zhou et al. (1997). Furthermore, in Cx46, cysteine substitutions of residues V44, A41, A40, and G38, which are homologous to residues A43, A40, A39, and V37 in Cx32*Cx43E1, were not modified by MTSET when the unapposed Cx46 hemichannel resides in the open state (Kronengold et al., 2003). In addition, cysteine substitutions of E42 and W45 (E41 and W44 in Cx32*Cx43E1) do not express membrane current in unapposed hemichannels formed by either connexin. The only difference in the behavior of cysteine substitutions of residues at the TM1/E1 border of Cx46 and Cx32*Cx43E1 is the ability of Cx46E43C to

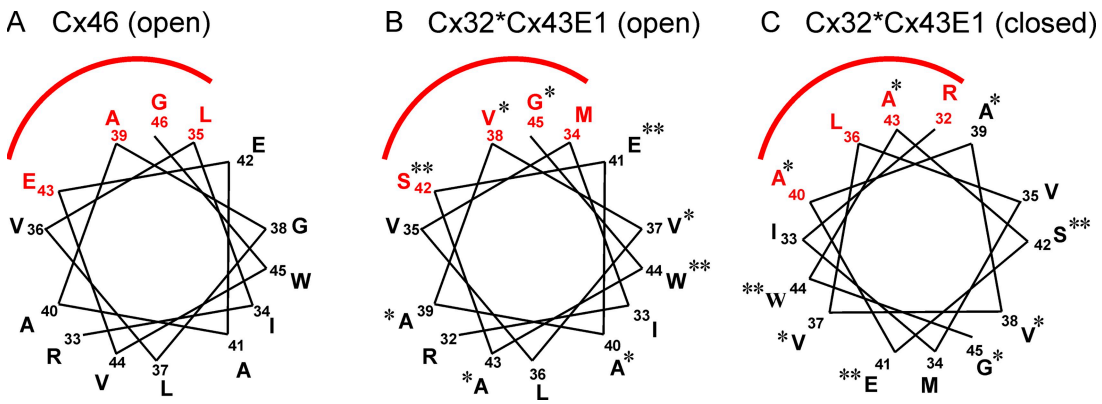

Figure 10. Helical wheel representation of reactive residues at the TM1/E1 border of Cx46 and Cx32*Cx43E1. (A) Helical wheel representation of residues R33 through G46 of Cx46. The residues span the TM1/E1 border, with residue E42 believed to be located on the membrane border. Residues accessible to MTS reagents applied to both the intercellular and extracellular face of the unapposed hemichannel are shown in red. These residues reside on one side of the helix, subtend an arc of ~80°, and line the pore of the open Cx46 unapposed hemichannel. Residue R33 is topmost in the figure, with the residue number increasing counterclockwise. Data are taken from Kronengold et al. (2003). (B) Helical wheel representation of homologous residues R32 through G45 of Cx32*Cx43E1 that line the pore of the open unapposed Cx32*Cx43E1 channel. Residues examined in this study are marked with asterisks. Two residues, V38C and G45C, react with MTSEA–biotin-X when the reagent is applied from either the intracellular or extracellular face of the channel and consequently are assigned as pore lining. Expression levels of S42C and E41C were insufficient to allow studies of accessibility to thiol modifying reagents, whereas W44C did not express membrane current. These residues are marked by two asterisks. (C) Helical wheel representation of the loop gate closed Cx32*Cx43E1 channel. The helical wheel pictured in B was rotated 140° clockwise to position residues A40C and A43C. This position accounts for the observed sensitivity of residues A40C and A43C to Cd^{2+} and their modification by bBBr when the channel is closed by loop gating (see Discussion).

express membrane currents while the homologous residue in Cx32*Cx43E1, S42C, does not. Collectively, these results indicate a substantial degree of similarity in the pore structure of Cx46 and Cx32*Cx43E1 in the vicinity of the TM1/E1 border.

The appearance of four to five stepwise changes in conductance of G45C and V38C after the application of MTSEA–biotin-X suggests that the pore diameter is large in the vicinity of these residues when the channel resides in the open state. To estimate the pore size of the open channel in the vicinity of residues V38 and G45, we constructed a molecular model of MTSEA–biotin-X that was geometry optimized in an aqueous periodic box with Hyperchem software. The modeled structure rendered with CPK spheres can be enclosed in a periodic box with minimum dimensions of 11.05 × 8.15 × 20.4 Å, giving a geometric mean dimension for this structure of 12.25 Å. Assuming hexagonal packing and modification of all six subunits, the minimal diameter of a pore that could accommodate six MTSEA–biotin-X molecules is ∼36 Å based on the geometric mean dimension of the thiol reagent (see Yu et al., 2009). However, it is likely that the pore diameter is somewhat smaller, probably in the range of 25 to 30 Å, as we most often observe four or five stepwise changes in conductance attributable to thiol reactions. The large pore size and lower affinity of cadmium ions for single cysteine residues could explain the small decrease (∼20%) in conductance that is observed when 10 µM Cd^{2+} is applied to open V38C and G45C channels. Presumably, these residues display low affinity monodentate interactions with Cd^{2+} when the channel resides in the open state, as the current reduction is readily reversed by washing with Cd^{2+}-free solutions.

Conformational changes associated with loop gating

Based on excised patch channel recordings, it does not appear that the A43C residue can react with MTSEA–biotin-X when the channel resides in the open state. However, in macroscopic records, this residue forms a high affinity cadmium binding site and reacts with the thiol-reactive bBBr at hyperpolarizing membrane potentials that are sufficient to close both the V_j and loop gate. These observations, combined with the failure to observe any inhibition of A43C currents by cadmium at moderate hyperpolarizing and depolarizing membrane potentials, conditions that strongly favor population of the open state of channel, support the view that the mechanism of Cd^{2+} block and bBBr modification is state dependent. Examinations of A43C channels on the N2E background, which reverses the gating polarity of the V_j gate, indicate that closure of the loop gate, not the V_j gate, is required for high affinity Cd^{2+} binding and bBBr accessibility. We propose that the closure of the loop gate results in a conformational change that provides accessibility of A43C residues to bBBr and that Cd^{2+} effectively locks the channel in the loop-gated closed conformation.

Studies of heteromeric A43C:Cx32*Cx43E1 channels suggest that the high affinity Cd^{2+} site involves at least four A43C residues and that the relative positions of coordinating residues may be important. Indeed, consideration of the electron configuration of Cd^{2+} ($[Kr]5s^04d^{10}$) indicates that coordination would most likely involve four or fewer cysteine residues (see also Vargek et al., 1999). Loussouarn et al. (2001) have shown that coordination of Cd^{2+} by cysteine mutations of Kir channels results from a tetrahedral organization of four cysteine-Sγ atoms coordinated to one central Cd^{2+}. In this geometry, 5-Å separations of Sγ atoms are optimal, although other coordination geometries involving fewer Sγ or other atoms in the cysteine or adjacent residues are possible (Belcastro et al., 2005, 2009). The ability of A43C residues to form disulphide bonds (at least in biochemical assays with channels closed by 5 mM Ca^{2+}) suggests that the channel can adopt a conformation that positions two Sγ atoms within ∼2 Å. Although the relationship of this conformation that can be tested only biochemically to the loop gate closed state observed electrophysiologically cannot be established directly, it is possible that they may be similar. It is important to note that the biochemical and electrophysiological studies were performed in different concentrations of external calcium. Oocytes were cultured in higher (5 mM) external calcium solutions for the biochemical assay to ensure their viability while attempting to maximize connexin channel expression. Verselis and Srinivas (2008) have shown that Cx46 currents are substantially reduced with increasing external Ca^{2+} and Mg^{2+} as a consequence of the stabilization of the closed loop gate conformation. If external Ca^{2+} has a similar effect on Cx32*Cx43E1 channels, it is possible that 5 mM Ca^{2+} may stabilize the loop gate closed conformation and promote the formation of disulfide bonds.

In the biochemical studies, no molecular weight forms larger than dimers are observed. This result indicates that disulfide bonding occurs between two of six available A43C residues in neighboring connexin subunits and supports the view that cysteines at other positions are not involved. Note that six cysteine residues can only form three pairs of dimers. If disulfide bonds were to form with cysteine residues at A43 and another native cysteine (CysX), one would expect that more than two subunits could be cross-linked, for example, the trimer A43C-CysX-A43C, the tetramer A43C-CysX-A43C-CysX, and larger oligomers could form.

The simplest mechanism to achieve a conformation that positions A43C residues into the channel pore in the closed state is by a clockwise rotation of each TM1 helix by ∼140° (Fig. 10 C). It should be noted that rotation by itself would not be sufficient to position the Sγ atoms of these cysteine residues within the distance

required to coordinate Cd^{2+} or form disulfide bonds. Recall that the pore diameter of the channel at the level of V38 and G45, residues that flank A43, is probably in the range of 25 to 30 Å, much greater than the ~5-Å separations of four A43C Sγ atoms that are optimal for Cd^{2+} coordination or ~2 Å for disulfide bond formation. We propose that in addition to rotation, either each connexin subunit or each individual TM1 helix tilts into the channel pore bringing A43C residues to within 2–5 Å when the loop gate is closed. We predict that additional conformational changes occur to prevent steric clashes among the extracellular domains of the six subunits when the channel is closed.

In this model, A40C residues would also rotate into pore (Fig. 10 C), but the resulting distance between Sγ atoms even after tilt must be too large to allow high affinity coordination of Cd^{2+}. This would account for the apparent low affinity of A40C channels to bind Cd^{2+} as indicated by the reversibility of the Cd^{2+} block of A40C channels after wash with cadmium-free solutions. The rotation would move residues V38 and G45 out of pore into the protein core, predicting inaccessibility of these residues to thiol modification reagents when the channel resides in a voltage loop-gated closed state, whereas V37 and A39 would move from one interhelical surface to another, explaining the absence of Cd^{2+} block and any effect of DTT and TPEN on open or closed V37C and A39C channels and the apparent failure of these residues to react with MTSEA–biotin-X in macroscopic recordings over a range of polarizations.

It is interesting to note that the results presented here differ from the results recently presented by Verselis et al. (2009) for Cd^{2+} coordination by cysteine substitutions of Cx50 channels. In Cx50, cysteine substitutions of two residues, F43 and G46 that line the pore of the open channel in the TM1/E1 region, appear to contribute in the formation of a high affinity Cd^{2+} site at hyperpolarizing membrane potentials that favor loop gate closure in low Ca^{2+} (0.2 mM) bath solutions. It remains to be established if the differences in the results reflect different conformational changes underlying a common voltage-dependent loop-gating mechanism in channels formed by Cx50 and Cx32*Cx43E1, a different closed conformation as a consequence of different amounts of Ca^{2+} used in the two studies, or if they reflect different voltage-dependent gating mechanisms in the two unapposed hemichannels that manifest themselves as similar appearing transitions.

In summary, the data presented here establish that the structure of the open Cx32*Cx43E1 unapposed hemichannel pore is very similar if not identical to that of Cx46 and Cx50 unapposed hemichannels in the vicinity of the TM1/E1 border. In addition, the conformational changes underlying loop gating, but not V_j gating, appear to involve a rotation of the TM1 helix and an inward tilt of either each of the six connexin subunits or TM1 helices that form the Cx32*Cx43E1 unapposed hemichannel.

Appendix

Before the publication of this paper, Maeda et al. (2009) reported the structure of the connexin 26 gap junction channel at 3.5 Å resolution. There is reasonably good agreement between the crystal structure and functional studies reported here and by Kronengold et al. (2003) that assign residues at the TM1/E1 border as pore lining, assuming that the crystal structure corresponds to the open state of the gap junction channel. Residue G45 lines the open pore of Cx26 gap junction and the corresponding substituted cysteine residue, G45C, is modified by MTSEA–biotin-X when the unapposed Cx32*Cx43E1 hemichannel resides in the open state. Residues A39, A40, and V43 are buried within the protein core of the open Cx26 gap junction channel in agreement with the results of the current study. There are some differences; notably, residue V37 is predicted to line the pore of the open Cx26 gap junction channel, whereas V37C does not appear to be modified by MTSEA–biotin-X; rather the neighboring residue, V38C, is modified. These differences may reflect a minor divergence in the structure of the gap junction channel from that of an unapposed hemichannel or may reflect conformational changes resulting from the incorporation of a cysteine residue at certain positions. The crystal structure of the Cx26 gap junction indicates a rather complex structure at the TM1/E1 border (Fig. 4 b in Maeda et al., 2009) that involves a substantial bend initiated in the vicinity of the 43rd residue and a transition from an approximate α-helical conformation of residues 34–42 in TM1 to a short 3–10 helix involving residues 43–48 in E1. Consideration of the crystal structure suggests a possible mechanism underlying channel closure by loop gating that involves a relaxation of the bend in the vicinity of the 43rd residues that could result in the formation of a constriction at the extracellular entrance of the channel pore and changes in the helical periodicity of the TM1/E1 segment that would be required to place the 40th and 43rd residues into the channel pore at the required distance to interact with Cd^{2+} when the unapposed Cx32*Cx43E1 channel resides in the closed conformation. This contrasts the simplistic model proposed in the current paper that involves a rotation and inward tilt of an α-helical TM1/E1 segment as depicted in Fig. 10. A similar change in the bend angle of the 43rd residue (44th residue in Cx50) could underlie the conformational change of the Cx50 unapposed hemichannel during loop gating as described by Verselis et al. (2009), suggesting that the basic mechanism of loop gating may be similar in the two unapposed hemichannels.

We thank Terrence Seales for technical support and Nir Ben-Tal and Sarel Fleishman for discussion.

This work was supported by National Institutes of Health grant GM46889 to T.A. Bargiello.

Edward N. Pugh Jr. served as editor.

Submitted: 23 January 2009
Accepted: 26 March 2009

REFERENCES

Bargiello, T.A., and P.R. Brink. 2009. Voltage-gating mechanisms of connexin channels. *In* Connexins: A Guide. A.L. Harris and D. Locke. Humana Press, New York. 103–128.

Belcastro, M., T. Marino, N. Russo, and M. Toscano. 2005. Interaction of cysteine with Cu^{2+} and group IIb (Zn^{2+}, Cd^{2+}, and Hg^{2+}) metal cations: a theoretical study. *J. Mass Spectrom.* 40:300–306.

Belcastro, M., T. Marino, N. Russo, and M. Toscano. 2009. The role of glutathione in cadmium ion detoxification: coordination modes and binding properties–a density functional study. *J. Inorg. Biochem.* 103:50–57.

Bezanilla, F. 2000. The voltage sensor in voltage-dependent ion channels. *Physiol. Rev.* 80:556–592.

Fleishman, S.J., V.M. Unger, M. Yeager, and N. Ben-Tal. 2004. A C^{α} model for the transmembrane α helices of gap junction intercellular channels. *Mol. Cell.* 15:879–888.

Harris, A.L., D.C. Spray, and M.V.L. Bennett. 1981. Kinetic properties of a voltage-dependent junctional conductance. *J. Gen. Physiol.* 77:95–117.

Kim, J.S., and R.T. Raines. 1995. Dibromobimane as a fluorescent crosslinking reagent. *Anal. Biochem.* 225:174–176.

Kronengold, J., E.B. Trexler, F.F. Bukauskas, T.A. Bargiello, and V.K. Verselis. 2003. Single channel SCAM identifies pore-lining residues in the first extracellular loop and first transmembrane domains of Cx46 hemichannels. *J. Gen. Physiol.* 122:389–405.

Krezel, A., W. Lesniak, M. Jezowska-Bojczuk, P. Mlynarz, J. Brasun, H. Kozlowski, and W. Bal. 2001. Coordination of heavy metals by dithiothreitol, a commonly used thiol group protectant. *J. Inorg. Biochem.* 84:77–88.

Krezel, A., R. Latajka, G.D. Bujacz, and W. Bal. 2003. Coordination properties of Tris(2-carboxyethyl)phosphine, a newly introduced thiol reductant, and its oxide. *Inorg. Chem.* 42:1994–2003.

Loussouarn, G., L.R. Phillips, R. Masia, T. Rose, and C.G. Nichols. 2001. Flexibility of the Kir6.2 inward rectifier K^{+} channel pore. *Proc. Natl. Acad. Sci. USA.* 98:4227–4232.

Maeda, S., S. Nakagawa, M. Suga, E. Yamashita, A. Oshima, Y. Fujiyoshi, and T. Tsukihara. 2009. Structure of the connexin 26 gap junction channel at 3.5 A resolution. *Nature.* 458:597–602.

Oh, S., C.K. Abrams, V.K. Verselis, and T.A. Bargiello. 2000. Stoichiometry of transjunctional voltage-gating polarity reversal by a negative charge substitution in the amino terminus of a connexin32 chimera. *J. Gen. Physiol.* 116:13–31.

Oh, S., S. Rivkin, Q. Tang, V.K. Verselis, and T.A. Bargiello. 2004. Determinants of gating polarity of a connexin 32 hemichannel. *Biophys. J.* 87:912–928.

Oh, S., V.K. Verselis, and T.A. Bargiello. 2008. Charges dispersed over the permeation pathway determine the charge selectivity and conductance of a Cx32 chimeric hemichannel. *J. Physiol.* 586:2445–2461.

Pantano, S., F. Zonta, and F. Mammano. 2008. A fully atomistic model of the Cx32 connexon. *PloS ONE.* 3:e2614.

Purnick, P.E., S. Oh, C.K. Abrams, V.K. Verselis, and T.A. Bargiello. 2000a. Reversal of the gating polarity of gap junctions by negative charge substitutions in the N-terminus of connexin 32. *Biophys. J.* 79:2403–2415.

Purnick, P.E., D.C. Benjamin, V.K. Verselis, T.A. Bargiello, and T.L. Dowd. 2000b. Structure of the amino terminus of a gap junction protein. *Arch. Biochem. Biophys.* 381:181–190.

Ri, Y., J.A. Ballesteros, C.K. Abrams, S. Oh, V.K. Verselis, H. Weinstein, and T.A. Bargiello. 1999. The role of a conserved proline residue in mediating conformational changes associated with voltage gating of Cx32 gap junctions. *Biophys. J.* 76:2887–2898.

Skerrett, I.M., J. Aronowitz, J.H. Shin, G. Cymes, E. Kasperek, F.L. Cao, and B.J. Nicholoson. 2002. Identification of amino acid residues lining the pore of a gap junction channel. *J. Cell Biol.* 159:349–359.

Suchyna, T.M., L.X. Xu, F. Gao, C.R. Fourtner, and B.J. Nicholson. 1993. Identification of a proline residue as a transduction element involved in voltage gating of gap junctions. *Nature.* 365:847–849.

Tombola, F., M.M. Pathak, and E.Y. Isacoff. 2006. How does voltage open an ion channel? *Annu. Rev. Cell Dev. Biol.* 22:23–52.

Trexler, E.B., M.V.L. Bennett, T.A. Bargiello, and V.K. Verselis. 1996. Voltage gating and permeation in a gap junction hemichannel. *Proc. Natl. Acad. Sci. USA.* 93:5836–5841.

Unger, V.M., N.M. Kumar, N.B. Gilula, and M. Yaeger. 1999. Three-dimensional structure of a recombinant gap junction membrane channel. *Science.* 283:1176–1180.

Vargek, M., X. Zhao, Z. Lai, G.L. McLendon, and T.G. Spiro. 1999. Monitoring cysteine and histidine ligands in zinc-finger peptides via ultraviolet resonance Raman spectroscopy. *Inorg. Chem.* 38:1372–1373.

Verselis, V.K. 2009. The connexin channel pore: pore-lining segments and residues. *In* Connexins: A Guide. A.L. Harris and D. Locke, editors. Humana Press, New York. 77–102.

Verselis, V.K., and M. Srinivas. 2008. Divalent cations regulate connexin hemichannels by modulating intrinsic voltage-dependent gating. *J. Gen. Physiol.* 132:315–327.

Verselis, V.K., C.S. Ginter, and T.A. Bargiello. 1994. Opposite voltage gating polarities or two closely related connexins. *Nature.* 368:348–351.

Verselis, V.K., M.P. Trelles, C. Rubinos, T.A. Bargiello, and M. Srinivas. 2009. Loop gating of connexin hemichannels involves movement of pore-lining residues in the first extracellular loop domain. *J. Biol. Chem.* 284:4484–4493.

Yeager, M., and A.L. Harris. 2007. Gap junction channel structure in the early 21st century: facts and fantasies. *Curr. Opin. Cell Biol.* 19:521–528.

Yu, A.S.L., M.H. Cheng, S. Angelow, D. Günzel, S.A. Kanzawa, E.E. Schneeberger, M. Fromm, and R.D. Coalson. 2009. Molecular basis for cation selectivity in claudin-2–based paracellular pores: identification of an electrostatic interaction site. *J. Gen. Physiol.* 133:111–127.

Zhou, Z.-W., A. Pfahnl, R. Werner, A. Hudder, A. Llanes, A. Luebke, and G. Dahl. 1997. Identification of a pore lining segment in gap junction hemichannels. *Biophys. J.* 72:1946–1953.